SYMPOSIUM REVIEW

# Biological validation of electron paramagnetic resonance (EPR) image oxygen thresholds in tissue

Inna Gertsenshteyn[1,2,3], Mihai Giurcanu[4], Peter Vaupel[5,6] and Howard Halpern[2,3]

[1]*Department of Radiology, University of Chicago, IL, USA*
[2]*Department of Radiation and Cellular Oncology, University of Chicago, Chicago, IL, USA*
[3]*Center for EPR Imaging In Vivo Physiology, University of Chicago, Chicago, IL, USA*
[4]*Department of Public Health Sciences, University of Chicago, IL, USA,*
[5]*Department of Radiation Oncology, Medical Center, University of Freiburg, Germany*
[6]*German Cancer Consortium (DKTK), Partner site Freiburg and German Cancer Research Center (DKFZ), Heidelberg, Germany*

Edited by: Laura Bennet & Janna Morrison

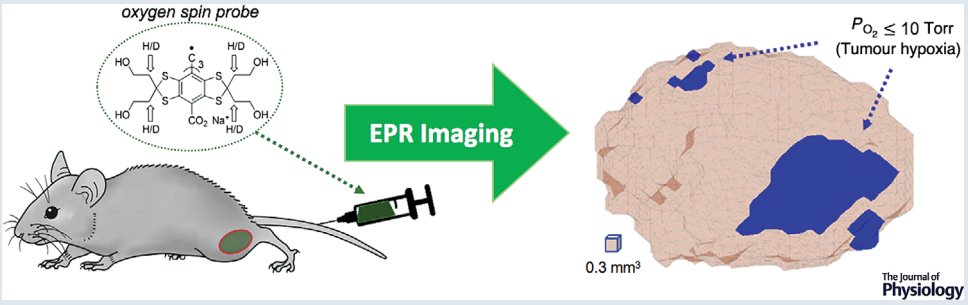


**Abstract** Measuring molecular oxygen levels *in vivo* has been the cornerstone of understanding the effects of hypoxia in normal tissues and malignant tumors. Here we discuss the advances in a variety of partial pressure of oxygen ($P_{O_2}$) measurements and imaging techniques and relevant oxygen thresholds. A focus on electron paramagnetic resonance (EPR) imaging shows the validation of treating hypoxic tumours with a threshold of $P_{O_2} \leq 10$ Torr, and demonstrates utility for *in vivo* oxygen imaging, as well as its current and future role in cancer studies.

(Received 12 February 2020; accepted after revision 26 May 2020; first published online 7 June 2020)
**Corresponding author** H. Halpern: Department of Radiation and Cellular Oncology, University of Chicago, Chicago, IL, USA. Email: h-halpern@uchicago.edu

**Abstract figure legend** Electron paramagnetic resonance (EPR) is a powerful tool for quantitative imaging of $P_{O_2}$ to study and treat tumour hypoxia. This example shows a preclinical tumour mouse model injected with an oxygen spin probe (OX063-$d_{24}$) into the tail vein for diffusion throughout the tumour, and the resulting hypoxic regions defined by $P_{O_2} \leq 10$ Torr obtained by EPR imaging.

**Inna Gertsenshteyn** received a BA in physics from Boston University in 2015. Upon graduation she joined inviCRO, now a Konica-Minolta Company, as an image analyst for drug development studies. In 2017, she joined the University of Chicago as a graduate student in medical physics. Her PhD dissertation with co-advisors Howard Halpern, MD, PhD, and Chin-Tu Chen, PhD, focuses on multimodal imaging of tumor hypoxia using PET, EPR and MR imaging. **Howard Halpern** is both a physicist in high energy physics and a physician in radiation oncology. He has directed major developments of EPR oxygen imaging and is Director of the NIH Centre for EPR Imaging *In Vivo* Physiology. Along with leaders in the field like Dr Peter Vaupel, Ms Gertsenshteyn and Dr Halpern are interested in the physiological effects of tumour hypoxia and how to best treat it.

This review was presented at the 'ISOTT 2019 oxygen transport to tissue' meeting, which took place in Albuquerque, New Mexico, USA, 28–31 July 2019.

 DOI: 10.1113/JP278816

The Journal of Physiology

## Introduction

For over a century, molecular oxygen concentrations in tissues and malignancies of living systems have been found to correlate with various anti-cancer treatment effects, beginning with radiation toxicity (Schwarz, 1909). Low oxygenation in all living systems results in resistance to radiation toxicity (Howard-Flanders, 1958; Thomlinson & Gray, 1955). The enormous complexity of living systems can confound such measurements since they depend on the intrinsic accuracy (i.e. oxygen resolution) of the measurements, the volume to which individual measurements are sensitive (spatial resolution), and the sources of confounding physiological variation that affect the measurement of the molecular oxygen concentrations. Imaging molecular oxygen content further complicates the process.

The partial pressure of oxygen ($P_{O_2}$) is an absolute measurement, with some uncertainty, of oxygen *in vivo*. As oxygen moves from the blood plasma (a source) to the mitochondria (a sink) by diffusion, a gradient is formed, with pressure lower at the sink than at the source (Wilson *et al.* 2006). The difference in $P_{O_2}$, and therefore the gradient, increases with the rate of oxygen consumption within a cell. While *in vitro* cellular measurements describe the 50% onset of radiation resistance to radiation at ∼2.5 Torr (= mmHg), *in vivo* tissue and tumour measurements have clustered about 10 Torr (Vaupel *et al.* 2007; Vaupel & Mayer, 2015). *In vivo*, malignant well-oxygenated cells have $P_{O_2}$ values between 10 and 60 Torr.

It is important not to assign a *universal* threshold of hypoxia to any tissues, cells, microvessels, etc. Relevant thresholds and their onsets vary depending on the physiological process being studied and how those measurements are taken, as demonstrated in Fig. 1. For example, *in vivo* experiments of tissue determine that critical $P_{O_2}$ is between 8 and 10 mmHg, while *in vitro* experiments on cytochromes determine 0.02–0.07 mmHg as the critical threshold. In addition, mean concentrations of ATP, PME, $P_i$ and pH rise and fall differently as a function of $P_{O_2}$ (Höckel & Vaupel, 2001).

Electron paramagnetic resonance (EPR) is a new imaging modality that accurately measures $P_{O_2}$, and has shown promising results to optimize preclinical oxygen image-guided radiation therapy. A goal of this article is to demonstrate the basics of EPR imaging and other oxygen imaging modalities such as positron emission tomography (PET), and the relevant $P_{O_2}$ thresholds in tissues.

## Measurement and imaging methods

### Fundamentals of EPR imaging

The relationships between energy, the magnetic moment, and the magnetic field are similar in electron paramagnetic resonance (EPR) and nuclear magnetic resonance (NMR) in their dependence on the particle mass. Because the mass of an electron is approximately three orders of magnitude smaller than the mass of a proton, the magnetic field strength of an EPR imager is reduced to 9–40 mTesla, rather than the 1.5–9.4 Tesla field strength used in magnetic resonance imaging (MRI). Therefore, EPR imagers are significantly lighter, more affordable to build and maintain, and have no possibility for harmful or even fatal accidents compared to MR imagers (Panych & Madore, 2018). Nevertheless, EPR $P_{O_2}$ imaging is accompanied by T2-weighted MRI, which provides high resolution anatomical contrast to define the boundaries of tumours, or other structures of interest, registered with the EPR $P_{O_2}$ images.

In MRI, the main magnetic field aligns the abundant water hydrogen nuclear spins in one direction as a net magnetization. Without this main magnetic field, the proton spins are randomly oriented. A second magnetic field disturbs the proton spins by a pulse of electromagnetic energy, which induces transitions between energy levels. Because the lower level has more members, there is a net absorption of energy creating a population excitation (Pooley, 2005).

A pulse response imager measures the time it takes for those disturbed spins to relax to their undisturbed orientations (also called the relaxation rate) over microsecond time intervals with 10's of kilohertz repetitions (Currie *et al.* 2013). The excitations take place in a series of magnetic field gradients, which causes the absorption to occur at different, identifiable locations and transforms that information into an image (Lauterbur, 1973; Bottomley & Andrew, 1978).

Unlike MRI, EPR imaging measures unpaired electron spins of dissolved and diffusible molecules (Gallez *et al.* 2004). These are scarce in biological systems since free metals like iron and copper catalyse chemical reactions. These transition metal unpaired electron spins are bound in carrying proteins or enzymes, and are not measurable at low EPR frequencies at biologically relevant temperatures (Epel & Halpern, 2013). *The exception is molecular oxygen* ($O_2$), which is free to diffuse in living tissues. $O_2$ bears two unpaired, rapidly relaxing electrons. The relaxation is too fast to directly measure; therefore, an oxygen spin probe must be introduced into the system in question (Gallez *et al.* 2004; Biller *et al.* 2011).

Each spin probe (e.g. OX063-$d_{24}$ in Fig. 2*A*) contains a relatively stable unpaired electron that interacts with the two unpaired electrons of oxygen molecules (Matsumoto *et al.* 2004). The EPR imager can detect the relaxation rates of the spin probes, and how their relaxation rates change in the presence or absence of oxygen (Bobko *et al.* 2009; Epel *et al.* 2014). There is a linear relationship between the relaxation rate of the spin probe and $P_{O_2}$, where low

$P_{O_2}$ corresponds to a low relaxation rate, and high $P_{O_2}$ corresponds to a high relaxation rate (Fig. 2*B*).

Overall, the signal-to-noise ratio (SNR) of the system varies with the number of spins in that voxel, and higher SNR leads to a higher spatial resolution of the image. Currently, the range of spatial resolution in EPR is 1–5 mm with the higher resolution at lower $P_{O_2}$.

In a 250-MHz (a low frequency) pulse EPR imager, a trityl spin probe (OX063-$d_{24}$) as shown in Fig. 2*A* is useful for oxygen imaging *in vivo* because of its strong signal and low toxicity (Kuzhelev *et al.* 2015; Epel *et al.* 2019). Once injected into the mouse tail vein, the probes diffuse in the extracellular fluid compartment of the tumour, where the clearance half-time is 20–30 min, while the clearance half-time in the blood stream is 2–5 min (Epel *et al.* 2010) due to enhanced permeability and retention (Maeda *et al.* 2000). The original *in vivo* pulse EPR $P_{O_2}$ imaging technique is due to the group of Murali Krisha at the National Cancer Institute (Bourg *et al.* 1993). Recent *in vivo* spectral spatial images using rapid scan EPR have been developed by the Khramtsov group at West Virginia University (Tseytlin *et al.* 2019).

Multiple projections of the spin probes' relaxation rates are acquired in the EPR imager to generate a three-dimensional image (Fig. 2*C*), where each voxel corresponds to a $P_{O_2}$ value. The heterogeneity of hypoxia within the tumour shows the importance of imaging the entire volume, rather than just one- or two-dimensional measurements (Williams *et al.* 2002). Fiducial-based registration of the EPR image to an anatomical CT or MRI image is necessary to define anatomical boundaries.

In general, EPR imaging has the advantage of a high quantitative accuracy, with uncertainty less than 1 Torr in the range of 1–10 Torr (Epel *et al.* 2014; Epel *et al.* 2019). This makes EPR imaging ideal in differentiating hypoxic *vs.* well-oxygenated regions. EPR imagers also have different penetration depth abilities depending on their frequency, which ranges from 0.2 to 1 GHz.

Imaging at a lower frequency, such as 250 MHz, has an 8 cm penetration depth (Roschmann, 1987), which is advantageous to quantitative imaging of larger animals (Halpern *et al.* 1994; Epel *et al.* 2010). High frequency EPR oximetry at 1.2 GHz has a penetration depth at 5–10 mm, which is limited to small animal imaging or peripheral anatomy (Swartz & Clarkson, 1998). The tradeoff, however, is that the sensitivity of an EPR instrument increases with increasing frequency as $\nu^{0.8}$ (Halpern *et al.*

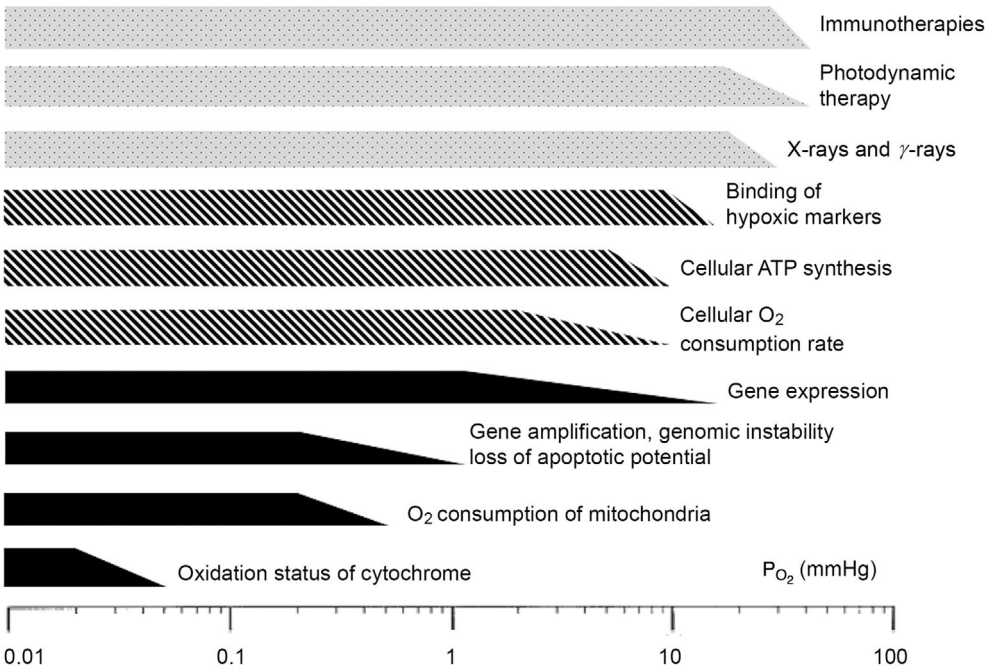


**Figure 1. Schematic of critical oxygen levels that characterize the onset of hypoxia**
Below these thresholds, functions of tissues, cells and organelles change. Filled bars represent mechanisms at the organelle and molecular levels; hatched bars represent cellular functions; open bars represent therapy forms. Reprinted with permission from the *Journal of the National Cancer Institute* (Höckel & Vaupel, 2001).

1994; Rinard *et al.* 2002), so the SNR is sacrificed for a higher penetration depth.

## $P_{O_2}$ measurement methods

It is possible to obtain a larger penetration depth (8 cm or more) with phosphorescence quenching at optical frequencies with a more invasive fiberoptic needle probe or a needle electrode. Both the OxyLite $P_{O_2}$ system (Oxford Optronics, UK) (Seddon *et al.* 2001) and the polarographic microelectrode measures a local $P_{O_2}$ (Braun *et al.* 2001).

Eppendorf polarographic needle electrodes measure $P_{O_2}$ within tissues, and have been integral in demonstrating the heterogeneity of oxygenation in human tumours (Höckel *et al.* 1991; Vaupel *et al.* 1991; Okunieff *et al.* 1993; Brizel *et al.* 1994). Eppendorf needle electrodes have also extensively been used to determine that, in tumour tissues, the threshold of 10 Torr predicted malignant progression in cervical cancer (Höckel *et al.* 1993, 1996). These studies emphasized the importance of personalized treatment of tumours, even 30 years ago. All these needle probes, however, are invasive and only obtain measurements of local $P_{O_2}$.

An optical method of imaging $P_{O_2}$ uses phosphorescence quenching of an infused porphyrin molecular sensor. The phosphorescent lifetimes of various probes were found to depend on the oxygen concentration (Vanderkooi *et al.* 1987). The advantages of oxygen measurements by phosphorescence includes millisecond response time with accuracy down to 0.1 Torr in low-oxygen pressures – a wide dynamic range, and applicable to *in vivo* tissue measurements (Wilson *et al.* 2006).

Using phosphorescence quenching, $P_{O_2}$ maps can be imaged in mice using pulsed trans-illumination. The phosphorescent probe decays over time, and the phosphorescence decay constant is calculated for each pixel fit to a single exponential. A two-dimensional $P_{O_2}$ image showed low $P_{O_2}$ values were present in the same tumour locations within the mouse (Wilson *et al.* 2006). This demonstration of quantifying and imaging oxygen is not in 3D, though tomographic imaging is theoretically possible (Apreleva *et al.* 2006).

The absorption of optical frequency limits this technique to window chamber models, invasive direct microscopy or images of very superficial structures.

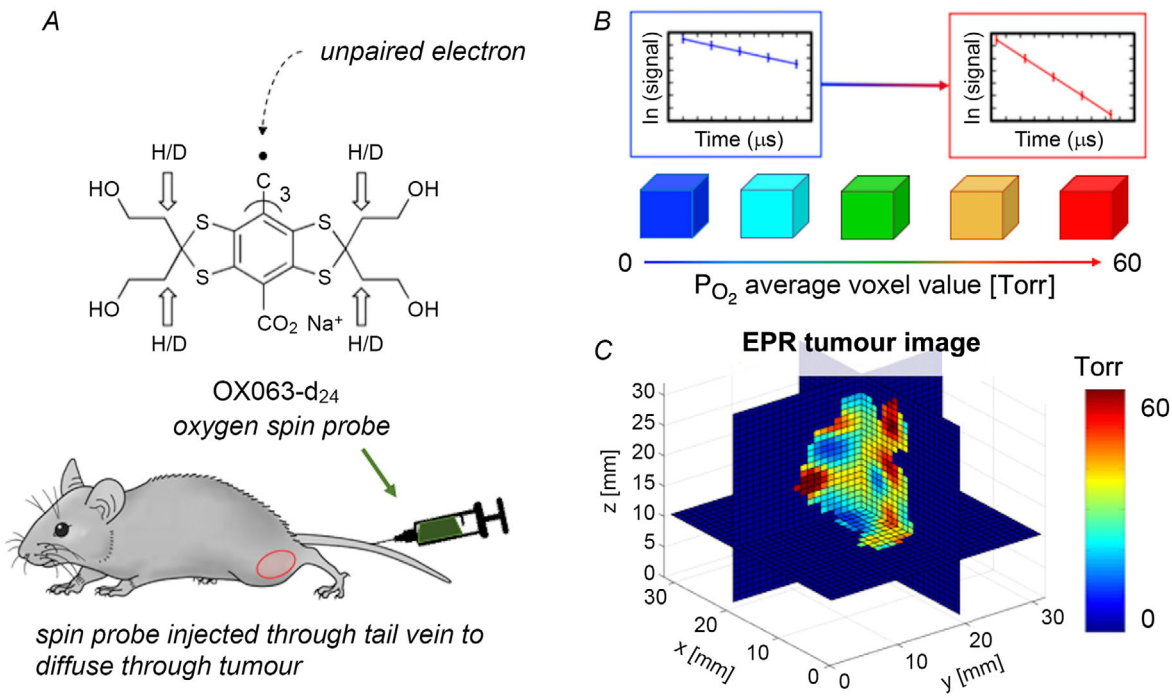


**Figure 2. Quantitative $P_{O_2}$ imaging with spin lattice relaxation EPR**
*A*, chemical structure of oxygen spin probe OX063-$d_{24}$, which is infused into the mouse via tail vein. *B*, in the EPR spin-lattice relaxation signal, the relaxation rate of the spin probe is higher for high $P_{O_2}$ and lower for low $P_{O_2}$. *C*, tomographic reconstruction shows a 3D quantitative distribution of $P_{O_2}$ in the tumour in isotropic voxels of $0.67 \times 0.67 \times 0.67$ mm$^3$, where $P_{O_2}$ voxels $\leq$ 10 Torr show hypoxia (blue).

### Qualitative hypoxia measurements with PET

Several radiotracers are available to image with PET to assess hypoxia, though the accuracy of these tracers has been questioned for decades. The threshold of uptake to identify hypoxic voxels varies greatly depending on several factors, including but not limited to the radiotracer's injection method, uptake unit, time imaged post-injection, and quality of the PET machine (Raleigh *et al.* 1996; Peeters *et al.* 2015; Silvoniemi *et al.* 2018).

One of the most widely used radiotracers for clinical cancer studies is $^{18}$F-fluoromisonidazole (FMISO), a nitroimidazole compound labelled with F-18. The F-18 radionuclide has a 110-min half-life, and the misonidazole biological half-life is 50 min (Jerabek *et al.* 1986; Grierson *et al.* 1989). Once the nitroimidazole enters a hypoxic cell, it can undergo reduction and consequent local molecular binding. This binds the nitroimidazole inside the cell. In normal well-oxygenated cells, the reduced nitro group can be oxidized back into the original substance by $O_2$ and diffuse away (Xu *et al.* 2017).

Within 2–4 h, FMISO accumulates in hypoxic cells and the radionuclide can be detected by PET imaging systems. FMISO has non-specific accumulation in normoxic colon tissues or no accumulation in pancreatic tumours, however, so FMISO is a tumour-type dependent radiotracer subject to confounding variation (Roels *et al.* 2008; Segard *et al.* 2013).

FMISO binds to hypoxic cells in the range between 2 and 10 Torr, because chronically hypoxic cells do not appear to retain the tracer (Rasey *et al.* 1987). There is also controversy between whether the pharmacokinetics and distribution of FMISO are affected by the immature and disorganized tumour microvasculature, which could also prevent the tracer from reaching hypoxic regions far from capillaries.

Early *in vitro* cell work showed a sigmoidal relationship between FMISO uptake and oxygen concentration, where uptake increased at low oxygen (Rasey & Evans, 1991). The point of inflection on this sigmoidal curve would indicate the threshold of hypoxia in terms of FMISO uptake and $P_{O_2}$ levels, which is currently under investigation at the Halpern laboratory in collaboration with the Kao laboratory in a home-built hybrid PET-EPR imaging system (Kim *et al.* 2019).

FMISO is used in clinical trials for imaging hypoxic tumours and planning radiation treatments based on the FMISO uptake. However, its clinical usefulness has not yet been shown to be significantly more effective than fluorodeoxyglucose (FDG), which accumulates in cells with high glucose metabolism. Distinction in titles is that EPR measured $pO_2$ quantitatively, while PET tracers accumulate in hypoxic cells. The image can be quantified in terms of standard uptake value (SUV), or the ratios of tumour to blood and muscle. Variation in PET imagers across and within institutions also contribute to a lack of standardization.

In a recent publication, the ratio of FMISO radioactivity levels in tumour to blood was found to be $1.43 \pm 0.50$ and $1.32 \pm 0.12$ at 2 and 4 h post-injection, respectively; the tumour to muscle ratio was $1.31 \pm 0.52$ and $1.12 \pm 0.30$ at 2 and 4 h (Masaki *et al.* 2015). Finally, a recent French FMISO consortium study found no benefit to directing increased radiation dose to hypoxic tumour regions defined using FMISO PET (Vera *et al.* 2017, 2019). This high variance hints at the extensive future work that must be done to determine whether there is an absolute threshold of FMISO uptake for treating tumour hypoxia as there is with EPR imaging ($P_{O_2} \leq 10$ Torr).

A major difference to keep in mind between the nitroimidazole for PET imaging, and the trityl spin probe imaged with EPR, is that the nitroimidazole binds intracellularly where the FMISO accumulates. In contrast, the spin probe diffuses in the tumour extracellularly and is simply measuring the relaxation rates of the exogenous spin probes in the presence or absence of oxygen. The extracellular localization may explain the lack of animal toxicity when using appropriate amounts for imaging.

## Relevance of thresholds for $P_{O_2}$ measurement and images

Determination of a threshold separating hypoxic from well oxygenated tissue or tumour regions is a bivariate process: either the tissue $P_{O_2}$ is above or below the threshold. This is similar to the process by which human X-rays are determined by a radiologist to be either normal or abnormal, the latter prompting either further radiographic study or medical intervention. This binary process originated during World War II using radar or sonar signals to separate benign objects from dangerous objects. It is commonly referred to as receiver operator characteristic (ROC) analysis (Metz, 1978).

One can apply a form of ROC analysis to a continuous characteristic of tissue, in this case the $P_{O_2}$ of each voxel within the image. A crucial component of ROC analysis is choosing a biologically relevant threshold of a property, e.g. local therapy resistance, the local level at which a hypoxia responsive protein is produced, therapy sensitivity, or the level at which the hypoxia responsive protein ceases.

The mathematical model of this situation assumes that there are two populations of voxels, each with its own distribution and $P_{O_2}$ values. It is assumed that there is an optimal $P_{O_2}$ threshold to distinguish between the two populations. In the case of using a $P_{O_2}$ image to define this, it is also assumed that there are macroscopic tissue regions of contiguous voxels that have the same property, such as radioresistance.

One can estimate the fraction of hypoxic voxels in core samples of tumour tissue for a given $P_{O_2}$ threshold using the EPR $P_{O_2}$ image, and measure the concentration of a hypoxia-associated protein such as the vascular endothelial growth factor (VEGF) in each biopsied sample (Elas *et al.* 2011). Plotting a curve of the fraction of regions included from the definition of hypoxia *vs.* the fraction included at a given level of hypoxia protein provides an example of the ROC curve.

A central parameter of ROC analysis is the area under the curve (AUC). Increased AUC describes a more significant distinction provided by the threshold and improved prediction accuracy.

In preliminary analysis of mouse core biopsy specimens, the selection of a $P_{O_2}$ threshold of 10 Torr provided the highest AUC correlation with hypoxia inducible factor-1 (HIF-1) in the core biopsy specimens. Interestingly, the AUC maximum for VEGF was 30 Torr, confirming previous analysis (Elas *et al.* 2011). Further development of applying ROC analysis to determine optimal thresholds for various hypoxia-related protein concentrations is ongoing.

## EPR oxygen imaging for cancer therapy

In the first complete study of radiation dose painting to treat hypoxic mammalian tumour regions with a boost of radiation, a low-frequency 250 MHz EPR imager with pulsed spin-lattice relaxation oxygen imaging was used to image $P_{O_2}$ (Epel *et al.* 2019). A threshold of $P_{O_2} \leq 10$ Torr was used to define tumour hypoxia.

Currently a typical human clinical treatment plan radiates an entire tumour with one or fractionated doses with homogeneous dose distribution. By applying a boost (extra radiation) to hypoxic cells with a higher dose, the treatment would spare healthy surrounding tissue. This is referred to as dose painting, and remains controversial in the field because of a history of increased radiation complication due to unnecessary 'hot spots' in the radiation dose distributions, particularly to critical structures necessary to maintain good quality of life.

Despite this clinical controversy, few preclinical experiments have tested the efficacy of dose painting hypoxic regions. Based on EPR oxygen images, the Halpern laboratory has radiated two randomized groups of similar distribution in tumour size and hypoxic fraction. In one group, a radiation boost was delivered to hypoxic tumour regions (Fig. 3*A*) compared to a boost of equal volumes to well-oxygenated tumour regions (Fig. 3*B*). Tumours were grown in the leg gastrocnemius muscle of C3H mice to radiobiologically relevant size for imaging and radiation treatment, and were observed for tumour recurrence. This study has been completed and published (Epel *et al.* 2019) in FSa fibrosarcoma tumour mouse models and repeated for confirmation in MCa4 mammary adenocarcinoma tumour mouse models (H. Halpern, in press).

These EPR studies demonstrated a significant increase in tumour control ($P < 0.05$) in two mammalian tumour types using Kaplan-Meier survival analysis, one of which has been published and is shown in Fig. 3*C* (Epel *et al.* 2019). Of note, the significant difference was obtained in a randomized experiment with a total of 54 animal

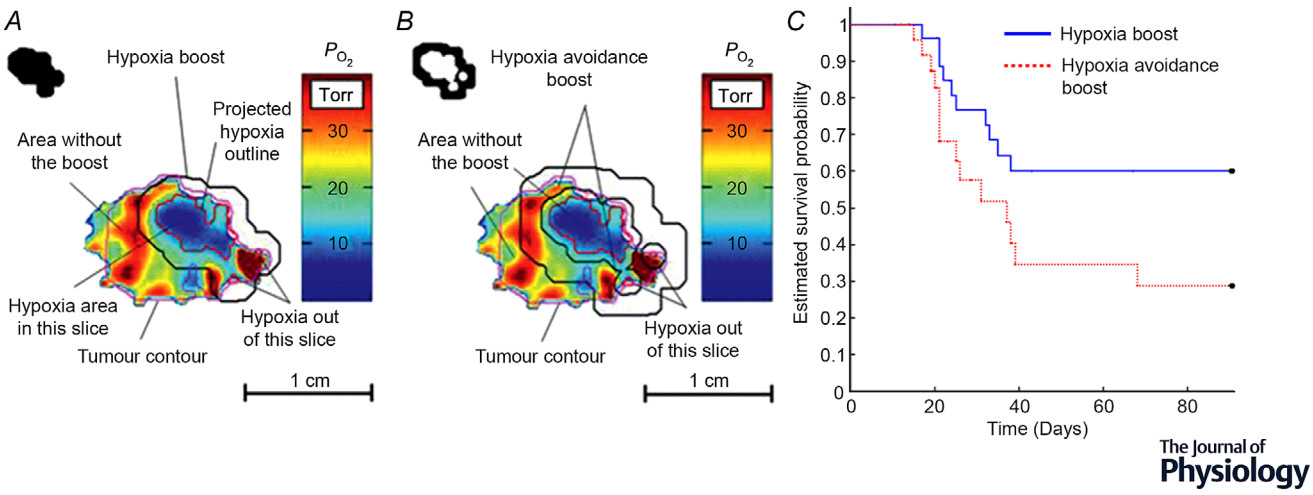


**Figure 3. Method and results boosting hypoxic or well oxygenated tumor form EPR $P_{O_2}$ images**
*A* and *B*, radiation treatment plans and delivery schemes for hypoxia boost (*A*) and hypoxia avoidance boost (*B*). The selected tumour slice is a quantitative $P_{O_2}$ map, as indicated by the colour bar. Upper left corners display the block shape apertures to deliver the dose beam. *C*, the resulting Kaplan-Meier survival (tumour recurrence) probability using a competing risk model with log-rank analysis for fibrosarcoma tumour mouse models, showing a significantly higher survival probability for hypoxia boost treatments ($P < 0.05$). Figure reproduced with permission from *International Journal of Radiation Oncology, Biology and Physics* (Epel *et al*. 2019).

subjects. This demonstrates the efficacy of dose painting by specifically targeting hypoxic tumour regions. In humans, these hypoxic regions are less likely to include the critical tissues and organs necessary to maintain a high degree of function.

In radiation treatment, >98% of hypoxia was targeted, with the dose map conforming to the heterogeneous hypoxic regions. A previous study that only targeted 85% of hypoxia failed, which underscores the strength of hypoxic cancer cells and the importance of accurately targeting them.

This work demonstrates a biological endpoint: improved local tumour control based on the EPR $P_{O_2}$ image. It is the first demonstration of improved control in a mammalian tumour after over a century of knowing about hypoxic resistance. It validates several issues including the use of the 10 Torr tumour threshold, the ability of EPR $P_{O_2}$ image to define it and finally, the effectiveness of delivery of the hypoxic boost within 2 h of obtaining the $P_{O_2}$ image.

## Conclusions

This year, *The Journal of Physiology* celebrates the passage of a century since Krogh published in *The Journal* his definition of the size of the drainage region of a capillary before onset of metabolism induced hypoxia and the definition of a $P_{O_2}$ threshold (Krogh, 1919).

As previously noted, there are several $P_{O_2}$ thresholds that have biologically relevant consequences. An important threshold is the onset of tumour resistance to cytotoxic tumour therapy, particularly radiation. EPR $P_{O_2}$ images appear to be, in two preclinical tumour models (Epel *et al.* 2019; H. Halpern, in press), able to define radiation resistant regions that with extra radiation doses improve tumour control relative to increased radiation to oxygenated tumour portions. That there are targetable macroscopic resistant regions in these preclinical models is of significance.

Much work remains to provide technology for human application and demonstration of the safety of the use of the spin probe in human subjects. If this is borne out, we must demonstrate the existence of such macroscopic, targetable regions in human tumours. Only then can we provide a major path to the improvement of the therapeutic index in radiation delivery.

## References

Apreleva SV, Wilson DF & Vinogradov SA (2006). Tomographic imaging of oxygen by phosphorescence lifetime. *Appl Opt* **45**, 8547–8559.

Bobko AA, Dhimitruka I, Eubank TD, Marsh CB, Zweier JL & Khramtsov VV (2009). Trityl-based EPR probe with enhanced sensitivity to oxygen. *Free Rad Bio and Medicine* **47**, 654–658.

Biller JR, Meyer V, Elajaili H, Rosen GM, Kao GPY, Eaton SS & Eaton GR (2011). Relaxation times and line widths of isotropically-substituted nitroxides in aqueous solution at X-band. *Magn Reson* **212**, 370–377.

Bottomley PA & Andrew ER (1978). RF Magnetic field penetration, phase shift and power dissipation in biological tissue: implications for NMR imaging. *Phys Med Biol* **23**, 630–643.

Bourg J, Krishna MC, Mitchell JB, Tschudin RG, Pohida TJ, Friauf WS, Smith PD, Metcalfe J, Harrington F & Subramanian S (1993). Radiofrequency FT EPR spectroscopy and imaging. *J Magn Reson* **103**, 112–115.

Braun RD, Lanzen JL, Snyder SA & Dewhirst MW (2001). Comparison of tumor and normal tissue oxygen tension measurements using OxyLite or micro-electrodes in rodents. *Am J Physiol Heart Circ Physiol* **280**, H2533–H2544.

Brizel DM, Rosner GL, Harrelson J, Prosnitz LR & Dewhirst MW (1994). Pretreatment oxygenation profiles of human soft tissue sarcomas. *Int J Radiat Oncol Biol Phys* **30**, 635.

Currie S, Hoggard N, Craven IJ, Hadjivassiliou M & Wilkinson ID (2013). Understanding MRI: basic MR physics for physicians. *Postgrad Med J* **89**, 209–223.

Elas M, Hleihel D, Barth ED, Haney CR, Ahn K-H, Pelizzari CA, Epel B, Weichselbaum RR, Halpern HJ (2011). Where it's at really matters: In situ in vivo vascular endothelial growth factor spatially correlates with electron paramagnetic resonance $p_{O_2}$ images in tumors of living mice. *Mol Imag Biol*, **13**, 1107–1113. https://doi.org/10.1007/s11307-010-0436-4.

Epel, B & Halpern, H (2013). Electron paramagnetic resonance oxygen imaging in vivo. *Electron Paramag Res*, **23**, 180–208.

Epel B, Bowman MK, Mailer C & Halpern HJ (2014). Absolute oxygen R-1e imaging in vivo with pulse electron paramagnetic resonance. *Magn Reson Med* **72**, 362–368.

Epel B, Haney CR, Hleihel D, Wardrip C, Barth ED & Halpern HJ (2010). Electron paramagnetic resonance oxygen imaging of a rabbit tumor using localized spin probe delivery. *Med Phys* **37**, 2553–2559.

Epel B, Maggio MC, Barth ED, Miller RC, Pelizzari CA, Krzykawska-Serda M, Sundramoorthy SV, Aydogan B, Weichselbaum RR, Tormyshev VM & Halpern HJ (2019). Oxygen-guided radiation therapy. *Int J Radiat Oncol Biol Phys* **103**, 977–984.

Gallez B, Baudelet C & Jordan BF (2004). Assessment of tumor oxygenation by electron paramagnetic resonance: principles and applications. *NMR Biomed* **17**, 240–263.

Grierson JR, Link JM, Mathis CA, Rasey JS & Krohn KA (1989). A radiosynthesis of fluorine-18 fluoromisonidazole. *J Nucl Med* **30**, 343–350.

Halpern HJ (2019). EPR molecular oxygen images identify biologically relevant tumor hypoxia in two mammalian models to increase tumor control [abstract]. In *Poster Session 3: Neuroscience, New Chemistry, Biology & Bioengineering Oncology*, 2nd Poster Award Nominee Presentations and Judging; 2019 Sept 3–7; WMIC, Montreal, Canada; Abstract nr P258.

Halpern HJ, Yu C, Peric M, Barth E, Grdina DJ & Teicher BA (1994). Oxymetry deep in tissues with low-frequency electron paramagnetic resonance. *Proc Natl Acad Sci U S A* **91**, 13047–13051.

Höckel M, Knoop C, Schlenger K, Vorndran B, Baussmann E, Mitze M, Knapstein PG, & Vaupel P (1993). Intratumoral $pO_2$ predicts survival in advanced cancer of the uterine cervix. *Radiother Oncol* **26**, 45–50.

Höckel M, Schlenger K, Aral B, Mitze M, Schäffer U & Vaupel P (1996). Association between tumor hypoxia and malignant progression in advanced cancer of the uterine cervix. *Cancer Res* **56**, 4509–4515

Höckel M, Schlenger K, Knoop C & Vaupel P (1991). Oxygenation of carcinomas of the uterine cervix: evaluation by computerized $O_2$ tension measurements. *Cancer Res* **51**, 6098-6102.

Höckel M & Vaupel P (2001). Tumor hypoxia: definitions and current clinical, biologic, and molecular aspects. *J Natl Cancer Inst* **93**, 266–276.

Howard-Flanders P (1958). Physical and chemical mechanisms in the injury of cells by ionizing radiation. *Adv Biol Med Phys* **6**, 553–603.

Jerabek PA, Patrick TB, Kilbourn MR, Dischino DD & Welch MJ (1986). Synthesis and biodistribution of 18F-labeled fluoronitroimidazoles: potential in vivo markers of hypoxic tissue. *Int J Appl Rad Isotopes* **37**, 599–605.

Kim H, Epel B, Sundramoorthy S, Tsai H-M, Barth E, Halpern H, Chen C-T, Kao C-M (2019). Development of a PET/EPRI simultaneous imaging system for assessing tumor hypoxia [abstract]. In *Instrumentation: New System Design and Emerging Technology II*; 2019 June 22–25; SNMMI, Anaheim, CA; Abstract nr 526.

Krogh A (1919). The supply of oxygen to the tissues and the regulation of the capillary circulation. *J Physiol* **52**, 457–474.

Kuzhelev AA, Trukhin DV, Krumkacheva OA, Strizhakov RK, Rogozhnikova OY, Troitskaya TI, Fedin MV, Tormyshev VM & Bagryanskaya EG (2015). Room-temperature electron spin relaxation of triarylmethyl radicals at the X- and Q-bands. *J Phys Chem B* **119**, 13630–13640.

Lauterbur P (1973). Image Formation by Induced Local Interactions: Examples employing nuclear magnetic resonance. *Nature* **242**, 190–191.

Maeda H, Wu J, Sawa T, Matsumura Y & Hori K (2000). Tumor vascular permeability and the EPR effect in macromolecular therapeutics: a review. *J Control Release* **65**, 271–284.

Masaki Y, Shimizu Y Yoshioka T, Tanaka Y, Nishijima K, Zhao S, Higashino K, Sakamoto S, Numata Y, Yamaguchi Y, Tamaki N & Kuge Y (2015) The accumulation mechanism of the hypoxia imaging probe "FMISO" by imaging mass spectrometry: possible involvement of low-molecular metabolites. *Sci Rep* **5**, 16802

Matsumoto K, English S, Yoo J, Yamada K, Devasahayam N, Cook JA, Mitchell JB, Subramanian S & Krishna MC (2004). Pharmacokinetics of a triarylmethyl-type paramagnetic spin probe used in EPR oximetry. *Magnet Reson Med* **52**:885–892.

Metz CE (1978). Basic principles of ROC analysis. *Seminars in Nuclear Medicine*, **8**, 283–298.

Okunieff P, Höckel M, Dunphy EE, Schlenger K, Knoop C & Vaupel P (1993). Oxygen tension distributions are sufficient to explain the local response of human breast tumors treated with radiation alone. *Int J Radiat Biol Oncol Phys* **26**, 631

Panych LP & Madore B (2018). The physics of MRI safety. *J Mag Res Im* **47**, 28–43.

Peeters SG, Zegers CM, Lieuwes NG, van Elmpt W, Eriksson J, van Dongen GA, Dubois L & Lambin P (2015). A comparative study of the hypoxia PET tracers [18F]HX4, [18F]FAZA, and [18F] FMISO in a preclinical tumor model. *Int J Radiat Oncol Biol Phys* **91**, 351–359.

Pooley RA (2005). Fundamental physics of MR imaging. *RadioGraphics* **25**, 1087–1099.

Raleigh JA, Dewhirst MW & Thrall DE (1996). Measuring tumor hypoxia. *Semin Radiat Oncol* **6**, 37–45

Rasey, JS & Evans, ML (1991). Detecting hypoxia in human tumors. Vaupel, Peter & Jain, RK, *Tumor Blood Supply and Metabolic Microenvironment: Characterization and Implications for Therapy (Funktionsanalyse Biologischer Systeme, 20)*. Gustav Fischer Verlag.

Rasey JS, Grunbaum Z, Magee S, Nelson NJ, Olive PL, Durand RE & Krohn KA (1987). Characterization of radiolabeled fluoromisonidazole as a probe for hypoxic cells. *Radiat Res* **111**, 292–304

Rinard GA, Quine RW, Eaton SS & Eaton GR (2002). Frequency dependence of EPR signal intensity, 250 MHz to 9.1 GHz. *J Magn Reson* **154**, 80–84.

Roels S, Slagmolen P, Nuyts J, Lee JA, Loeckx D, Maes F, Stroobants S, Penninckx F & Haustermans K (2008) Biological image-guided radiotherapy in rectal cancer: is there a role for FMISO or FLT, next to FDG? *Acta Oncol* **47**, 1237–1248.

Roschmann P (1987). Radiofrequency penetration and absorption in the human body: limitations to high-field whole-body nuclear magnetic resonance imaging. *Med Phys* **14**, 922–931.

Schwarz G (1909) Uber Desensibilisierung gegen Rontgen- und Radiumstrahlen. *Munchner Medizinishe Wochenschrift* **56**, 1217–1218.

Seddon BM, Honess DJ, Vojnovic B, Tozer GM & Workman P (2001). Measurement of tumor oxygenation: *in vivo* comparison of a luminescence fiber-optic sensor and a polarographic electrode in the p22 tumor. *Radiat Res* **155**, 837–846.

SegardT, Robins PD, Yusoff IF, Ee H, Morandeau L, Campbell EM, Francis RJ (2013). Detection of hypoxia with 18F-fluoromisonidazole (18F-FMISO) PET/CT in suspected or proven pancreatic cancer. *Clin Nucl Med*, **38**, 1–6. https://doi.org/10.1097/rlu.0b013e3182708777.

Silvoniemi A, Suilamo S, Laitinen T, Forsback S, Löyttyniemi E, Vaittinen S, Saunavaara V, Solin O, Grönroos TJ & Minn H (2018). Repeatability of tumour hypoxia imaging using [18F]EF5 PET/CT in head and neck cancer. *Eur J Nucl Med Mol Imaging* **45**, 161–169.

Swartz HM & Clarkson RB (1998). The measurement of oxygen in vivo using EPR techniques. *Phys Med Biol* **43**, 1957–1975.

Thomlinson RH & Gray LH (1955). The histological structure of some human lung cancers and the possible implications for radiotherapy. *Br J Radiol* **9**, 539–563.

Tseytlin O, Guggilapu P, Bobko AA, Al Ahmad H, Xu X, Epel B, O'Connell R, Hoblitzell EH, Eubank TD, Khramtsov VV, Driesschaert B, Kazkaz E & Tseytlin M (2019). Modular imaging system: Rapid scan EPR at 800 MHz. *J Magn Reson* **305**, 94–103.

Vanderkooi JM, Maniara G, Green TJ & Wilson DF (1987). An optical method for measurement of dioxygen concentration based upon quenching of phosphorescence. *J Biol Chem* **262**, 5476–5482.

Vaupel P, Höckel M & Mayer A (2007). Detection and characterization of tumor hypoxia using $pO_2$ histography. *Antioxid Redox Signal* **9**, 1221–1235.

Vaupel P & Mayer A (2015). The clinical importance of assessing tumor hypoxia: relationship of tumor hypoxia to prognosis and therapeutic opportunities. *Antioxid Redox Signal* **22**, 878–880.

Vaupel P, Schlenger K, Knoop C & Höckel M (1991). Oxygenation of human tumors: evaluation of tissue oxygen distribution in breast cancers by computerized $O_2$ tension measurements. *Cancer Res* **51**, 3316–3322.

Vera P, Mihailescu SD, Lequesne J, Modzelewski R, Bohn P, Hapdey S, Pépin LF, Dubray B, Chaumet-Riffaud P, Decazes P, Thureau S & all investigators of RTEP5 study (2019). Radiotherapy boost in patients with hypoxic lesions identified by (18)F-FMISO PET/CT in non-small-cell lung carcinoma: can we expect a better survival outcome without toxicity? [RTEP5 long-term follow-up]. *Eur J Nucl Med Mol Imaging* **46**, 1448–1456.

Vera P, Thureau S, Chaumet-Riffaud P, Modzelewski R, Bohn P, Vermandel M, Hapdey S, Pallardy A, Mahé MA, Lacombe M, Boisselier P, Guillemard S, Olivier P, Beckendorf V, Salem N, Charrier N, Chajon E, Devillers A, Aide N, Danhier S, Denis F, Muratet JP, Martin E, Riedinger AB, Kolesnikov-Gauthier H, Dansin E, Massabeau C, Courbon F, Farcy Jacquet MP, Kotzki PO, Houzard C, Mornex F, Vervueren L, Paumier A, Fernandez P, Salaun M & Dubray B (2017). Phase II study of a radiotherapy total dose increase in hypoxic lesions identified by 18F-Misonidazole PET/CT in patients with non-small cell lung carcinoma (RTEP5 Study). *J Nucl Med* **58**, 1045–1053.

Wilson DF, Lee WM, Makonnen S, Finikova O, Apreleva S & Vinogradov SA (2006). Oxygen pressures in the interstitial space and their relationship to those in the blood plasma in resting skeletal muscle. *J Appl Physiol* **101**, 1648–1656.

Williams BB, al Hallaq H, Chandramouli GV, Barth ED, Rivers JN, Lewis M, Galtsev VE, Karczmar GS & Halpern HJ (2002). Imaging spin probe distribution in the tumor of a living mouse with 250 MHz EPR: correlation with BOLD MRI. *Magn Reson Med* **47**, 634–638.

Wilson DF, Vinogradov S, Lo L-W & Huang L (2006). Oxygen dependent quenching of phosphorescence: a status report. *Adv Exp Med Biol* **388**, 101–107.

Xu Z, Li X-F, Zou H, Sun X & Shen B (2017). 18F-Fluoromisonidazole in tumor hypoxia imaging. *Oncotarget* **8**, 94969–94979.

## Additional information

### Competing interests

US patents 8,664,955 B1, 9,392,957 B1, 10,551,450 B2, and 10,568,537 B2 were recently awarded to H.H., who is also a member of a start-up company O2M to market to $P_{O_2}$ imaging technology. Other authors have no competing interests.

### Author contributions

I.G. and H.H. designed this work and wrote the manuscript with contributions by M.G. and P.V. of analysis and interpretation of concepts for the work. All authors have either drafted or critically revised the work. All authors have approved the final version of the manuscript, and agree to be accountable for all aspects of the work reviewed in ensuring that questions related to the accuracy or integrity of any part of the work are appropriately investigated and resolved. All authors qualify for authorship, and all those who qualify for authorship are listed.

### Funding

This work was supported by the National Institute of Biomedical Imaging and Bioengineering grant numbers T32 EB002103 and P41 EB002034, and by the National Cancer Institute grant numbers R01 CA236385, R01 CA098575, and P30 CA014599.

### Acknowledgements

We would like to thank Mellissa Grana for her proofreading and suggestions in this report.

### Keywords

electron paramagnetic resonance, hypoxia, oxygen sensing